Photoacoustics 36 (2024) 100585

Contents lists available at ScienceDirect

Photoacoustics

journal homepage: www.elsevier.com/locate/pacs

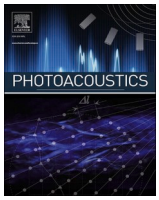

Carbon monoxide impurities in hydrogen detected with resonant photoacoustic cell using a mid-IR laser source

Chaofan Feng [a,b,d], Xiaowen Shen [a,b], Biao Li [c], Xiaoli Liu [a,b], Yujing Jing [a,b], Qi Huang [a,b], Pietro Patimisco [a,d,e], Vincenzo Spagnolo [a,d,e,*], Lei Dong [a,b,d,*], Hongpeng Wu [a,b,d,*]

[a] State Key Laboratory of Quantum Optics and Quantum Optics Devices, Institute of Laser Spectroscopy, Shanxi University, Taiyuan 030006, China
[b] Collaborative Innovation Center of Extreme Optics, Shanxi University, Taiyuan 030006, China
[c] Chongqing Key Laboratory of Optoelectronic Information Sensing and Transmission Technology, School of Optoelectronic Engineering, Chongqing University of Posts and Telecommunications, Chongqing 400065, China
[d] PolySense Lab—Dipartimento Interateneo di Fisica, University and Politecnico of Bari, Bari, Italy
[e] PolySense Innovations Srl, Bari, Italy

ARTICLE INFO

Keywords:
Resonant photoacoustic cell
Carbon monoxide
Hydrogen
Fuel cells

ABSTRACT

We report on a photoacoustic sensor system based on a differential photoacoustic cell to detect the concentration of CO impurities in hydrogen. A DFB-QCL laser with a central wavelength of 4.61 μm was employed as an exciting source with an optical power of 21 mW. Different concentrations of CO gas mixed with pure hydrogen were injected into the photoacoustic cell to test the linear response of the photoacoustic signal to the CO concentration. The stability of the long-term operation was verified by Allan-Werle deviation analysis. The minimum detection limit (MDL, SNR=1) results 8 ppb at 1 s and reaches a sub-ppb level at 100 s of integration time. Dynamic response of the system is linear and has been tested up to the concentration of 6 ppm. Saturation conditions are expected to be reached for CO concentration larger than 100 ppm.

1. Introduction

To address global climate change, 192 countries, almost every nation in earth, had signed a legally binding climate agreement "The Paris Agreement" [1,2]. In September 2020, China announced its goal vision of peaking carbon emissions before 2030 and achieving carbon neutrality by 2060 ("3060 target") [3]. To reduce carbon emissions, from the technical perspective, reducing the use of high carbon emitting energy sources such as oil and coal will be an impact strategy. Therefore, hydrogen energy, as a pollution-free and efficient energy source, is gradually receiving widespread attention [4]. In this context, fuel cells, as a type of hydrogen energy cell, have significant prospects for development.

Fuel cells mainly utilize hydrogen to operate, and large-scale pure hydrogen preparation and storage costs are relatively high. Currently, most hydrogen energy for fuel cells mainly comes from hydrocarbons reforming, which uses catalytic reactions to convert hydrocarbons into hydrogen [5–12]. Each year, around 6% of the world's natural gas and 2% of its coal is used to make grey hydrogen [13]. In the process of reforming hydrogen, there are inevitably the production of impurities, such as CO, NH_3, H_2S, etc. and any impurities present in hydrogen gas may result in substantial degradation of fuel cells. Indeed, the presence of these impurities can cause damage even when they are present at very low concentration levels (parts per billion (ppb)). Among impurities, CO has the most severe impact [14]. Platinum, recognized as the best catalyst for hydrogen oxidation reactions (HORs) and oxygen reduction reactions (ORRs) in acidic environments, is widely used in fuel cells. CO will closely bind to the Pt anodes, resulting in a decrease in active sites for hydrogen absorption and oxidation, which greatly reduces the performance of the fuel cell [5,9,15,16]. The voltage lose in the fuel cell will reach 85% when the cell is exposed to a CO content of 70 part-per-million (ppm) for 6 h [17]. It has been demonstrated that the CO concentration for Pt anodes needs to be less than 10 ppm, and for Pt-Ru anodes the CO concentration needs to be below 100 ppm to ensure good performance and long lifetime of fuel cells [5,18,19]. Therefore, there is a huge request for sensitive techniques for the detection of CO in hydrogen.

Existing analytical methods suitable for measuring ISO 14687

* Corresponding authors at: State Key Laboratory of Quantum Optics and Quantum Optics Devices, Institute of Laser Spectroscopy, Shanxi University, Taiyuan 030006, China
E-mail addresses: vincenzoluigi.spagnolo@poliba.it (V. Spagnolo), donglei@sxu.edu.cn (L. Dong), wuhp@sxu.edu.cn (H. Wu).

https://doi.org/10.1016/j.pacs.2024.100585
Received 3 October 2023; Received in revised form 8 January 2024; Accepted 9 January 2024
Available online 18 January 2024

impurities in fuel cell graded hydrogen mainly involve techniques based on gas chromatography and spectroscopy [20,21]. Cavity-enhanced Raman spectroscopy has been proposed as approach for detection of gaseous impurities in hydrogen and sub-ppm CO detection limit with measurement time of 60 s has been achieved [22]. Continuous wave cavity ring-down spectroscopy (CRDS) is also employed for detection of CO impurities in hydrogen and a commercial system provided by Tiger Optics (HALO 3 CO) reached a detection limit of 50 ppb with response time less than 1 min [23], in the range 0–2500 ppm. A more sensitive systems is also available from Tiger Optics (HALO MAX QCL CO) capable to reach 200 ppt detection limit with response time less than 1 min, but the response saturates for CO concentration larger than 500 ppb.

In recent years, photoacoustic spectroscopy (PAS) has received more and more attention among the optical gas sensing techniques. PAS exploits the photoacoustic effect occurring in gas enclosed within a resonant acoustic cell. The laser beam passes through the acoustic cell: photons are absorbed by the molecules via a resonant optical transition from the ground state to the excited state. Due to the instability of the excited state, the gas molecules will return to the ground state again through non-radiative transitions, with a consequent release of energy. If the laser beam is intensity-modulated, the gas molecules exhibit periodic expansions and contractions, resulting in the generation of sound waves. The concentration of the analyte can be retrieved by analyzing the acoustic signal. PAS technology in 2*f* configuration provides zero background and the signal results proportional to the laser power. In addition, PAS does not require an optical detector, moreover a sound detector is wavelength insensitive [24–28]. In 2015, a 2.3 μm continuous wave laser was employed to build a quartz enhanced photoacoustic spectroscopy (QEPAS) system to measure CO gas, and the final detection sensitivity was 43.3 ppm [29]. In 2020, Bo Sun achieved a 10 ppb CO detection at 10 s of integration time by using a T-shaped tuning fork, but only detected CO in sulfur hexafluoride (SF_6) [30], while in 2022, Hayden and co-authors demonstrated a CO sensor capable to reach part-per-trillion detection limit using an intracavity QEPAS approach [31]. Also in 2022, Sgobba et al. realized a very compact CO sensor for environmental monitoring exploiting the QEPAS approach and demonstrated its operation in a real urban environment [32].

In this work, a photoacoustic sensor with a resonant photoacoustic cell was demonstrated for the detection of CO in hydrogen. A CO absorption line located at 4.61 μm was selected. The working pressure and modulation depth of the sensor were optimized to maximize the sensitivity. The linearity of the response was demonstrated by calibrating the sensor with different concentrations of CO in hydrogen. We demonstrated the achievement of a minimum detection limit of 8 ppb at 600 torr, for an integration time of 1 s. The stability of the sensor during long-term operation was verified by Allan-Werle deviation analysis.

2. Experiment system

To roughly estimate the resonance frequency of the PAS cell when filled with H_2 or N_2, the resonance frequency f of the first-order longitudinal resonant mode of a photoacoustic cell can be simply expressed as [33]:

$$f = \frac{v}{2L} \tag{1}$$

where L is the effective length of the resonator and v is the speed of sound. The propagation speed of sound is related to the medium. When the sound propagates in a gas mixture, the speed of sound can be described as:

$$v = \sqrt{\frac{\kappa R_0 T}{\sum_1^n M_n C_n}} \tag{2}$$

where κ is an adiabatic index, R_0 is the molar gas constant, T is the temperature, n is the type of mixed gas, M_n and c_n are the molar mass and the concentration of the n-th analyte in the mixture, respectively. By substituting Eq. 2 in Eq. 1, the explicit dependence of the resonance frequency on the properties of analytes contained in a gas mixture can be retrieved:

$$f = \sqrt{\frac{\kappa R_0 T}{\sum_1^n M_n C_n}}\ \frac{1}{2L} \tag{3}$$

The estimated resonance frequency of the photoacoustic cell when filled with pure nitrogen or pure hydrogen can be easily calculated by using in Eq. 3 for the molar gas constant $R_0 = 8.314$ J/mol·K and or H_2 and N_2 the parameters listed in Table 1.

With a resonator length of 90 mm, the calculated resonance frequencies are 1922.8 Hz and 7219.9 Hz for pure nitrogen and pure hydrogen, respectively.

According to the *HITRAN* database [35], the strongest CO absorption band falls in the mid infrared region between 4.5 μm and 5.1 μm, as shown in Fig. 1.

Being the photoacoustic signal proportional to the intensity of the gas absorption line, the concentration of the gas to be measured, and the power of the laser, the strongest absorption feature free from any interference effect must be selected within the absorption bands. The absorption line with a central wavenumber of 2169.2 cm^{-1} and a line-strength of 4.5×10^{-19} cm/mol was selected because spectrally free from the main atmospheric interferents, such as water and carbon dioxide. The sketch of the PAS sensor setup is shown in Fig. 2.

A DFB-QCL (AdTech Optics, Model HHL-17–62) with a central wavelength of 4.61 μm was selected as the excitation light source. A current controller (ILX Light wave, Model LDX-3220) and a temperature controller (Thorlabs, Model TED 200 C) was used to regulate the wavelength of the laser, ensuring that the wavelength of the laser can target the selected CO gas absorption line. At a working temperature of 38.5 ℃ and a laser current of 210 mA, the laser wavelength matched the CO selected absorption resonance peak with an optical power of 21 mW. A sine wave and a triangular wave were generated through a dual channel function generator (Tektronix, Model AFG 3022) as the modulation signal and scanning signal of the laser, respectively. The frequency of the sine wave was set to half of the resonance frequency of the photoacoustic cell when filled with pure hydrogen, in second harmonic (2 *f*) and wavelength modulation approach. The triangular wave has a high and low level of 223 mA and 197 mA, respectively, with a scanning frequency of 10 mHz, which can ensure that the laser can fully scan the selected CO gas absorption line. At the same time, the function generator will trigger the lock-in amplifier (Stanford Research Systems, Model SR830), which is used to demodulate the electrical signal transmitted from the microphone to the lock-in amplifier. The differential photoacoustic cell had two identical cylindrical acoustic resonators, with a length of 90 mm and a diameter of 8 mm. At both ends of the acoustic resonator, there were two buffer volumes to suppressed flow velocity noise and window noise. Two electret condenser microphones (Primo Microphones Inc., Japan, model EM258) were placed at the center of the acoustic resonators, corresponding to its antinode location, where the sound pressure was highest. The sound wave signal generated by the photoacoustic effect was detected by the microphone and converted into an electrical signal, then amplified and transmitted to the lock-in amplifier. The demodulated signal was finally sent to the computer and further processed in a LabView program to retrieve the gas

Table 1
Adiabatic index κ and Molar mass *M* of pure nitrogen and pure hydrogen at atmospheric pressure and room temperature as reported on NIST database [34].

Buffer gas	Adiabatic index κ	molar mass of the gas *M* (Kg/mol)
N_2	1.4	0.028
H_2	1.41	0.002

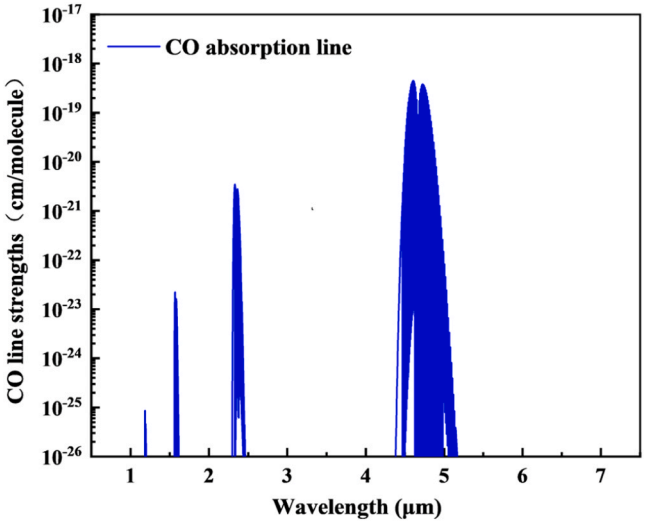

Fig. 1. The main absorption bands of CO molecules in the infrared region.

concentration. The power meter was used to monitor the output power of the laser in real time and for alignment purposes.

The gas handling system, composed by two needle valves, a pressure meter (MKS Instrument, Model 649B), a flow meter (Alicat Scientific, Model M-2SLPM-D/5 M) and a vacuum pump (Oerlikon Leybold Vacuum Inc., Model D16C), was used to measure and fix the pressure and the gas flow rate inside the PAS cell. Starting from a certified concentration of 10 ppm CO gas in H_2 and a cylinder with pure hydrogen, different concentrations of CO were obtained by using a gas dilution system (Environics, Model EN4000).

To measure the resonance frequency of the first-order longitudinal resonant mode of the photoacoustic cell when filled with nitrogen and hydrogen, 10 ppm CO in N_2 and in pure H_2 were injected into the photoacoustic cell, respectively. The laser output wavelength was locked at the peak of the targeted absorption line of CO gas at 4.61 μm, and the frequency of the QCL modulation signal was scanned nearby 1922.8 Hz and 7219.9 Hz, namely the predicted resonance frequencies in N_2 and H_2, respectively. To lock the laser wavelength on the CO absorption peak we implemented a 3 *f* wavelength locking technology, by using a gas reference cell positioned after the PAS cell in the system (not shown in Fig. 2). The two measured resonance curves are shown in Fig. 3.

From the resonance curves, the peak frequencies of 1779.8 Hz and 7048.9 Hz can be extracted when the cell is filled with nitrogen and hydrogen, respectively. Both values differ of less than 8% from the calculation predictions. These discrepancies can be ascribed to rough approximations in the model proposed in Eq. 3, which it does not take into account of the gas viscosity, the roughness of the internal walls of the cell and deviations in geometry between the modeled and the real cell. From both resonance curves, Q factor can be calculated as the ratio between the peak frequency and the full-width half-maximum value of the resonance curve, resulting 47 and 31 for nitrogen and hydrogen, respectively.

3. Results and discussion

A certified concentration 10 ppm of CO in H_2 (CO:H_2) gas was injected into the photoacoustic cell to optimize the operating conditions. The photoacoustic signal depends on the current modulation depth: the photoacoustic signal is maximized when the wavelength modulation depth is equal to linewidth of the absorption feature. Since the linewidth is pressure-dependent, the modulation depth that maximizes the PAS signal is expected to be related to the operating pressure. Fig. 4 reports the PAS signal as a function of modulation depth, for seven different pressure values spanning from 100 Torr to 670 Torr.

The highest PAS signal was obtained with a modulation depth of 70 mV at an operating pressure of 600 torr. All following measurements were performed at these operating conditions.

As representative, the PAS spectrum achieved for 10 ppm of CO:H_2 under the optimized operating conditions is shown in Fig. 5. The acquired signal exhibits a second harmonic derivative line-shape with a residual amplitude modulation contribution [36], arising from the direct intensity modulation of the laser, leading to an asymmetry of the two negative lobes.

The peak signal results 364 μV. Considering the 1σ noise level of 0.29 μV, a signal-to-noise ratio (SNR) of ~1255 can be estimated at 10 ppm, giving a minimum detection limit of ~8 ppb at SNR = 1.

To verify the linearity of the PAS sensor, different concentrations of

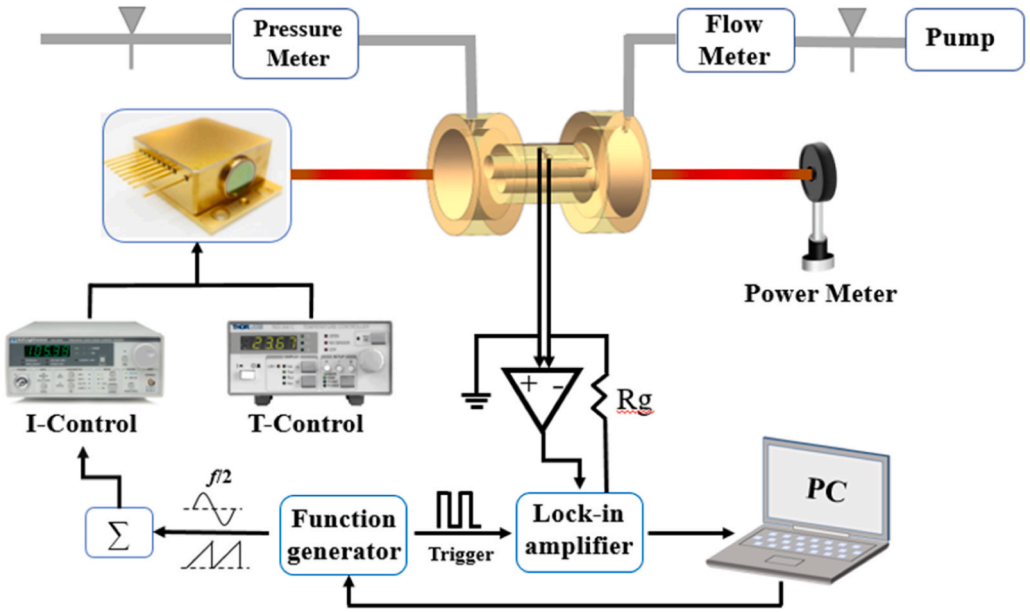

Fig. 2. Schematic of the CO sensor setup based on a differential resonance photoacoustic cell with a DFB-QCL exciting source. PC: personal computer; I-Control: current controller; T-Control: temperature controller.

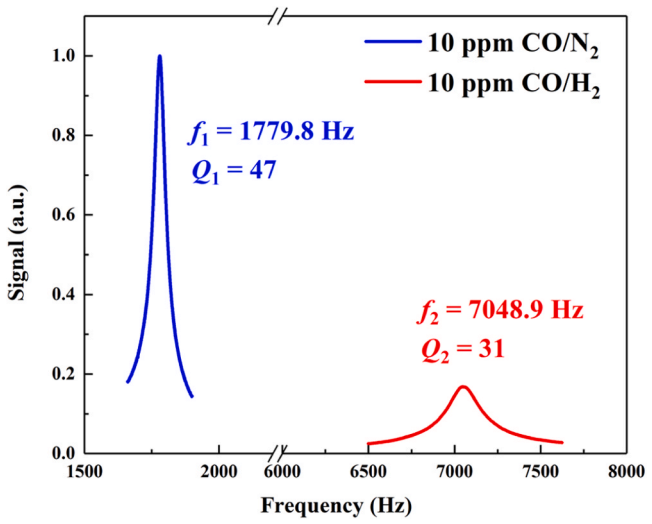

Fig. 3. Resonance frequency response curve of the photoacoustic cell under the concentration of 10 ppm CO in N_2 (blue) and H_2 (red).

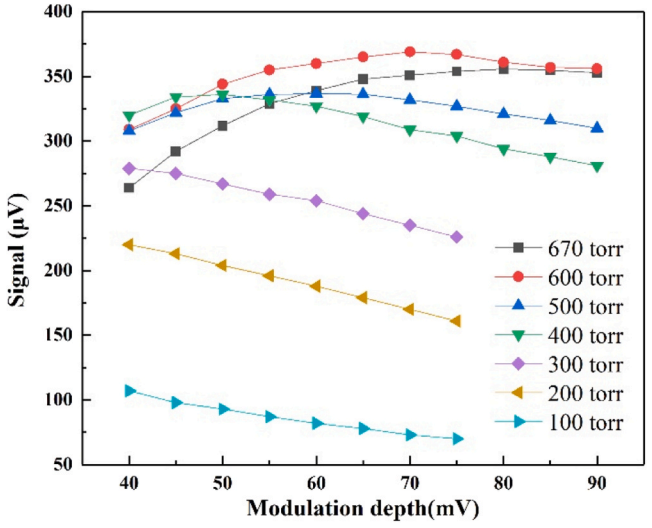

Fig. 4. The relationship between the photoacoustic signal and the modulation depth at different operating pressures. The experimental data were obtained at room temperature, with an integration time of 1 s and a flow rate of 100 sccm.

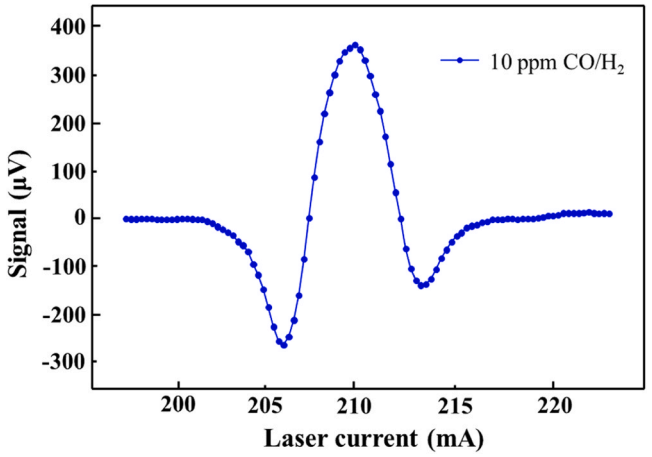

Fig. 5. PAS Spectral scan measured for 10 ppm of CO:H_2 with a modulation depth of 70 mV at an operating pressure of 600 torr.

CO:H_2 (from 200 ppb to 6 ppm) were generated by mixing the certified mixture of 10 ppm of CO:H_2 with pure hydrogen in different proportions, using the gas dilution system. With the emission wavelength of the QCL locked at the peak of the CO gas absorption line, we performed step scan measurements and 200 datapoints were collected for each CO concentration and plotted as a function of time in Fig. 6a. For each concentration, the average value was estimated and plotted as a function of CO concentration in Fig. 6b, together with the best linear fit of the experimental data. An R-square value of the linear fitting of 0.999 confirms a very good correlation between the observed outcomes and the observed predictor values. A sensitivity of 27.5 μV/ppm, i.e., the slope of the linear fit, was achieved and a mean PAS signal of 5.47 μV was obtained with a CO concentration of 200 ppb. Considering the 1σ noise level of 0.22 μV (standard deviation over 200 data points), a signal-to-noise ratio (SNR) of ~25 can be estimated at 200 ppb, giving a minimum detection limit of ~8 ppb at SNR = 1.

The long-term stability of the PAS sensor was verified by performing an Allan-Werle deviation analysis at 600 torr. Pure hydrogen was injected into the photoacoustic cell while the wavelength of the laser was locked at the peak of the CO absorption line, and the lock-in amplifier integration time was set to 1 s. The Allan deviation plot in ppb-unit is reported in Fig. 7. The behavior in the first part of the Allan Plot can be attributed to laser instability. After 100 s the signal decreases as $1/\sqrt{(t)}$ and the white noise remains the dominant noise source. With an integration time of 100 s, the ultimate detection limit reaches a value of ~ 0.7 ppb.

4. Conclusion

A photoacoustic sensor for measuring CO gas in H_2 was demonstrated in this work. The sensor used a differential photoacoustic cell as a detection element. A strong absorption line located at 4.61 μm was selected to enhance the detection sensitivity. The operating pressure and modulation depth were optimized, and the optimal values resulted 600 torr and 70 mV, respectively. The linear response of the sensor was investigated by generating different concentrations of CO in H_2 using the gas dilution system. The experimental results showed that the sensor can reach the minimum detection limit of 8 ppb at an integration time of 1 s, which reduces below 1 ppb at integration time larger than 1 min. Dynamic response of the system is linear and has been tested up to the concentration of 6 ppm and saturation conditions are expected for concentration larger than 100 ppm. Based on the fuel quality requirements specified by ISO/DIS 14687–2 and ISO/WD 14687–3 (August 2011), maximum impurity concentrations of CO are 0.2 ppm (Types I & II Grade D) and 10 ppm (Type I Grade E), respectively. Thereby, our sensor could represent an efficient tool to monitor the quality of the H_2 fuel in real world applications.

CRediT authorship contribution statement

Feng Chaofan: Writing – original draft, Investigation, Formal analysis, Conceptualization. **Shen Xiaowen:** Investigation, Conceptualization. **Wu Hongpeng:** Writing – review & editing, Writing – original draft, Supervision, Methodology, Conceptualization. **Spagnolo Vincenzo:** Writing – review & editing, Supervision, Conceptualization. **Li Biao:** Methodology, Conceptualization. **Liu Xiaoli:** Investigation, Conceptualization. **Jing Yujing:** Software, Investigation. **Dong Lei:** Writing – review & editing, Supervision, Project administration, Methodology. **Huang Qi:** Software, Methodology, Conceptualization. **Patimisco Pietro:** Writing – review & editing, Writing – original draft, Conceptualization.

Declaration of Competing Interest

The authors declare that they have no known competing financial interests or personal relationships that could have appeared to influence

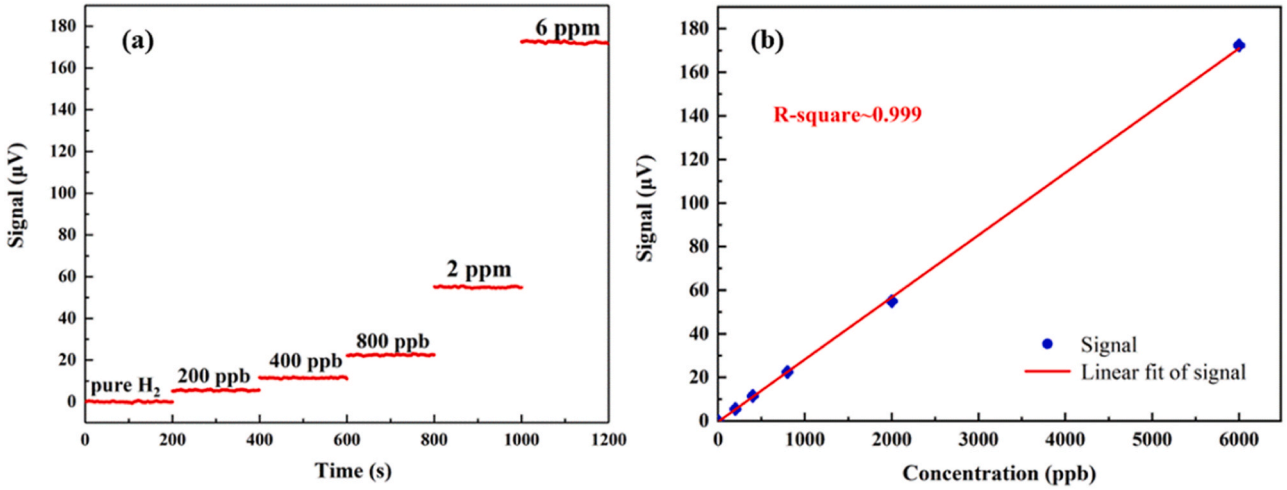

Fig. 6. (a) Photoacoustic signals at different CO concentrations. 200 datapoints were collected at each concentration. (b) Linear response of the photoacoustic signal and the concentration of CO gas. The 200 datapoints collected at each concentration were averaged (blue dots) and the red line represents the best-linear fitting curve of the average data. The error bars falls within the blue dots and the root-mean-square of the residuals results 0.95 μV.

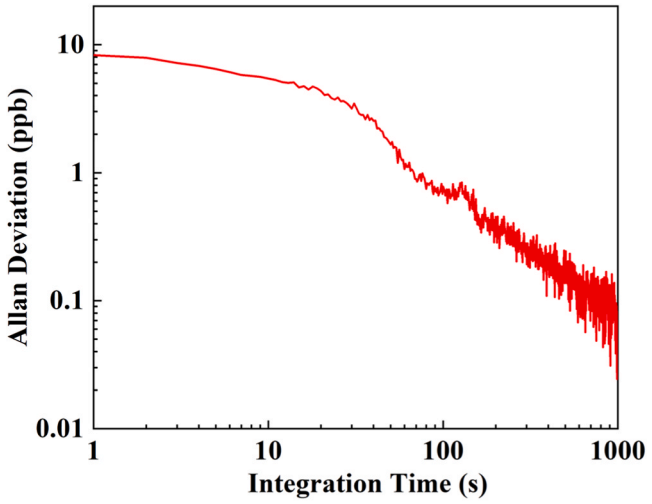

Fig. 7. Allan-Werle deviation as a function of the integration time. The experiment was carried out at room temperature under the operating pressure of 600 torr.

the work reported in this paper.

Data availability

Data will be made available on request.

Acknowledgements

This work was supported by National Natural Science Foundation of China (NSFC) (Nos. 62122045, 62075119 , 62235010 , 62175137); National Key R&D Program of China, code: 2019YFE0118200; The High-end Foreign Expert Program (Nos. G2023004005L); The Shanxi Science Fund for Distinguished Young Scholars (20210302121003). The authors from Dipartimento Interateneo di Fisica di Bari acknowledge financial support from PNRR MUR project PE0000021-NEST and THORLABS GmbH within the PolySenSe joint research laboratory.

References

[1] A. Savaresi, The Paris agreement: a new beginning? J. Energy Nat. Resour. Law 34 (2016) 16–26.
[2] C.F. Schleussner, J. Rogelj, M. Schaeffer, T. Lissner, R. Licker, E.M. Fischer, R. Knutti, A. Levermann, K. Frieler, W. Hare, Science and policy characteristics of the Paris Agreement temperature goal, Nat. Clim. Change 6 (9) (2016) 827–835.
[3] X. Wang, Y. Liu, J. Bi, M. Liu, New challenges of the Belt and Road Initiative under China's "3060" carbon target, J. Clean. Prod. 376 (2022) 134180.
[4] K. Sopian, W.R. Wan Daud, Challenges and future developments in proton exchange membrane fuel cells, Renew. Energy 31 (5) (2006) 719–727.
[5] C. Molochas, P. Tsiakaras, Carbon monoxide tolerant Pt-based electrocatalysts for H_2-PEMFC applications: current progress and challenges, Catalysts 11 (2021) 1127.
[6] E.D. Park, D. Lee, H.C. Lee, Recent progress in selective CO removal in a H_2-rich stream, Catal. Today 139 (4) (2009) 280–290.
[7] N. Zamel, X. Li, Effect of contaminants on polymer electrolyte membrane fuel cells, Prog. Energy Combust. Sci. 37 (3) (2011) 292–329.
[8] Y. Matsuda, T. Shimizu, S. Mitsushima, Adsorption behavior of low concentration carbon monoxide on polymer electrolyte fuel cell anodes for automotive applications, J. Power Sources 318 (2016) 1–8.
[9] X. Cheng, Z. Shi, N. Glass, L. Zhang, J. Zhang, D. Song, Z.-S. Liu, H. Wang, J. Shen, A review of PEM hydrogen fuel cell contamination: Impacts, mechanisms, and mitigation, J. Power Sources 165 (2) (2007) 739–756.
[10] M. Krumpelt, T.R. Krause, J.D. Carter, J.P. Kopasz, S. Ahmed, Fuel processing for fuel cell systems in transportation and portable power applications, Catal. Today 77 (1) (2002) 3–16.
[11] A.F. Ghenciu, Review of fuel processing catalysts for hydrogen production in PEM fuel cell systems, Curr. Opin. Solid State Mater. Sci. 6 (2002) 389–399.
[12] C. Song, Fuel processing for low-temperature and high-temperature fuel cells: challenges, and opportunities for sustainable development in the 21st century. Catal. Today 77 (1) (2002) 17–49.
[13] ⟨https://www.iea.org/reports/the-future-of-hydrogen⟩.
[14] J. Zhang, H. Wang, D.P. Wilkinson, D. Song, J. Shen, Z.-S. Liu, Model for the contamination of fuel cell anode catalyst in the presence of fuel stream impurities, J. Power Sources 147 (1-2) (2005) 58–71.
[15] S. Delgado, T. Lagarteira, A. Mendes, Air bleeding strategies to increase the efficiency of proton exchange membrane fuel cell stationary applications fuelled with CO ppm-levels, Int. J. Electrochem. Sci. 15 (1) (2020) 613–627.
[16] Y. Li, X. Wang, B. Mei, Y. Wang, Z. Luo, E. Luo, X. Yang, Z. Shi, L. Liang, Z. Jin, Z. Wu, Z. Jiang, C. Liu, W. Xing, J. Ge, Carbon monoxide powered fuel cell towards H_2-onboard purification, Sci. Bull. 66 (2021) 1305–1311.
[17] S. Jimenez, J. Soler, R.X. Valenzuel, L. Daza, Assessment of the performance of a PEMFC in the presence of CO, J. Power Sources 151 (2005) 69–73.
[18] P. Garbis, C. Kern, A. Jess, Kinetics and reactor design aspects of selective methanation of CO over a Ru/γ-Al2O3 catalyst in CO_2/H_2 rich gases, Energies 12 (3) (2019) 469.
[19] R. Peters, J. Meißner, Gasaufbereitung für Brennstoffzellen, Chem. Ing. Tech. 76 (10) (2004) 1555–1558.
[20] A. Murugan, A.S. BrownReview, of purity analysis methods for performing quality assurance of fuel cell hydrogen, Int. J. Hydrog. Energy 40 (11) (2015) 4219–4233.
[21] C. Beurey, B. Gozlan, M. Carré, T. Bacquart, A. Morris, N. Moore, K. Arrhenius, H. Meuzelaar, S. Persijn, A. Rojo, A. Murugan, Review and survey of methods for analysis of impurities in hydrogen for fuel cell vehicles according to ISO 14687: 2019, Front. Energy Res. 8 (2019) 615149.

[22] Pinyi Wang, Weigen Chen, Jianxin Wang, Yongkang Lu, Zijie Tang, Yaxiong Tan, Cavity-Enhanced Raman Spectroscopy for Detection of Trace Gaseous Impurities in Hydrogen for Fuel Cells, Anal. Chem. 95 (17) (2023) 6894–6904.
[23] ⟨https://www.ankersmid.com/AutoFiles/doc/6372_HALO_3_CO.pdf⟩.
[24] K. Chen, B. Zhang, S. Liu, F. Jin, M. Guo, Y. Chen, Q. Yu, Highly sensitive photoacoustic gas sensor based on multiple reflections on the cell wall, Sens. Actuators A Phys. 290 (2019) 119–124.
[25] Y. Ma, Y. He, Y. Tong, X. Yu, F. Tittel, Quartz-tuning-fork enhanced photothermal spectroscopy for ultra-high sensitive trace gas detection, Opt. Express 26 (2018) 32103–32110.
[26] A. Sampaolo, P. Patimisco, M. Giglio, A. Zifarelli, H. Wu, L. Dong, V. Spagnolo, Quartz-enhanced photoacoustic spectroscopy for multi-gas detection: a review, Anal. Chim. Acta 1202 (2021) 338894.
[27] K. Liu, X. Guo, H. Yi, W. Chen, W. Zhang, X. Gao, Off-beam quartz-enhanced photoacoustic spectroscopy, Opt. Lett. 34 (2009) 1594–1596.
[28] M. Giglio, A. Zifarelli, A. Sampaolo, G. Menduni, A. Elefante, R. Blanchard, C. Pfluegl, M.F. Witinski, D. Vakhshoori, H. Wu, V.M.N. Passaro, P. Patimisco, F. K. Tittel, L. Dong, V. Spagnolo, Broadband detection of methane and nitrous oxide using a distributed feedback quantum cascade laser array and quartz-enhanced photoacoustic sensing, Photoacoustics 17 (2020) 100159.
[29] Y. Ma, G. Yu, J. Zhang, X. Yu, R. Sun, Sensitive detection of carbon monoxide based on a QEPAS sensor with a 2.3 μm fiber-coupled antimonide diode laser, J. Opt. 17 (2015) 055401.
[30] B. Sun, A. Zifarelli, H. Wu, S.D. Russo, S. Li, P. Patimisco, L. Dong, V. Spagnolo, Mid-Infrared Quartz-Enhanced Photoacoustic Sensor for ppb-Level CO Detection in a SF6 Gas Matrix Exploiting a T-Grooved Quartz Tuning Fork, Anal. Chem. 92 (20) (2020) 13922–13929.
[31] J. Hayden, M. Giglio, A. Sampaolo, V. Spagnolo, B. Lendl, Mid-infrared intracavity quartz-enhanced photoacoustic spectroscopy with pptv – Level sensitivity using a T-shaped custom tuning fork, Photoacoustics 25 (2022) 100330.
[32] F. Sgobba, A. Sampaolo, P. Patimisco, M. Giglio, G. Menduni, A.C. Ranieri, C. Hoelzl, H. Rossmadl, C. Brehm, V. Mackowiak, D. Assante, E. Ranieri, V. Spagnolo, Compact and portable quartz-enhanced photoacoustic spectroscopy sensor for carbon monoxide environmental monitoring in urban areas, Photoacoustics 25 (2022) 100318.
[33] C. Feng, M. Giglio, B. Li, A. Sampaolo, P. Patimisco, V. Spagnolo, L. Dong, H. Wu, Detection of hydrogen sulfide in sewer using an erbium-doped fiber amplified diode laser and a gold-plated photoacoustic cell, Molecules 27 (2022) 6505.
[34] National Institute of Standards and Technology, ⟨https://webbook.nist.gov/⟩.
[35] I.E. Gordon, L.S. Rothman, R.J. Hargreaves, R. Hashemi, E.V. Karlovets, F. M. Skinner, et al., The HITRAN2020 molecular spectroscopic database, J. Quant. Spectrosc. Radiat. Transf. 277 (2022) 107949.
[36] P. Patimisco, A. Sampaolo, Y. Bidaux, A. Bismuto, M. Schott, J. Jiang, A. Muller, J. Faist, F.K. Tittel, V. Spagnolo, Purely wavelength- and amplitude-modulated quartz-enhanced photoacoustic spectroscopy, Opt. Express 24 (2016) 25943–25954.

Chaofan Feng is now pursuing a Ph.D. degree in atomic and molecular physics in the Institute of Laser Spectroscopy of Shanxi University, China. His research interests include gas sensors, photoacoustic spectroscopy, and laser spectroscopy techniques.

Xiaowen Shen is now pursuing a Ph.D. degree in atomic and molecular physics in the Institute of Laser Spectroscopy of Shanxi University, China. Recently, Her research has focused on the development of gas sensors , photoacoustic spectroscopy, photothermal spectroscopy and laser spectroscopy techniques.

Biao Li is now pursuing a Ph.D. degree in atomic and molecular physics in the Institute of Laser Spectroscopy of Shanxi University, China. His research interests include gas sensors, photoacoustic spectroscopy, and laser spectroscopy techniques.

Xiaoli Liu is now pursuing a Ph.D. degree in atomic and molecular physics in the Institute of Laser Spectroscopy of Shanxi university, China. Her research interests include gas sensor and photoacoustic spectroscopy.

Yujing Jing is now pursuing a professional master's degree in the Institute of Laser Spectroscopy at Shanxi University, China. Her research interests include gas sensors, photoacoustic spectroscopy, and laser spectroscopy techniques.

Qi Huang is now pursuing a master of Electronic Information in the Institute of Laser Spectroscopy of Shanxi University, China. Her research interests include gas sensors, photoelectric signal detection and processing, and tunable diode laser absorption spectroscopy.

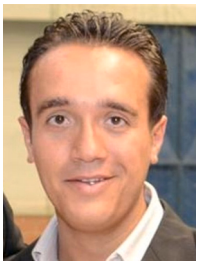

Prof. Pietro Patimisco obtained the Master degree in Physics (cum laude) in 2009 and the PhD Degree in Physics in 2013 from the University of Bari. Since 2023, he is an associate professor at the Physics Department of University of Bari. He was a visiting scientist in the Laser Science Group at Rice University in 2013 and 2014. The main scientific skills of Pietro Patimisco are related to the development of spectroscopic techniques for studying the light-matter interaction in the infrared range. Prof. Pietro Patimisco is co-founder of "PolySenSe Innovations", a company devoted to the development of optical-based sensors.

Vincenzo Spagnolo received the degree (summa cum laude) and the PhD, both in physics, from University of Bari. He works as Full Professor of Applied Physics at the Technical University of Bari. In 2019, he become Vice-Rector of the Technical University of Bari, deputy to Technology Transfer. Since 2017, he is the director of the joint-research lab PolySense, created by THORLABS GmbH and Technical University of Bari, devoted to the development and implementation of novel gas sensing techniques and the realization of highly sensitive QEPAS trace-gas sensors.

Lei Dong received his Ph.D. degree in optics from Shanxi University, China, in 2007. From June, 2008 to December, 2011, he worked as a post-doctoral fellow in the Electrical and Computer Engineering Department and Rice Quantum Institute, Rice University, Houston, USA. Currently he is a professor in the Institute of Laser Spectroscopy of Shanxi University. His research interests include optical sensors, trace gas detection, photoacoustic spectroscopy and laser spectroscopy.

Hongpeng Wu received his Ph.D. degree in atomic and molecular physics from Shanxi University, China, in 2017. From September, 2015 to October, 2016, he studied as a joint Ph.D. student in the Electrical and Computer Engineering Department and Rice Quantum Institute, Rice University, Houston, USA. Currently he is a professor in the Institute of Laser Spectroscopy of Shanxi University. His research interests include gas sensors, photoacoustic spectroscopy, photothermal spectroscope and laser spectroscopy techniques.